Journal of Materials Chemistry A

Accepted Manuscript

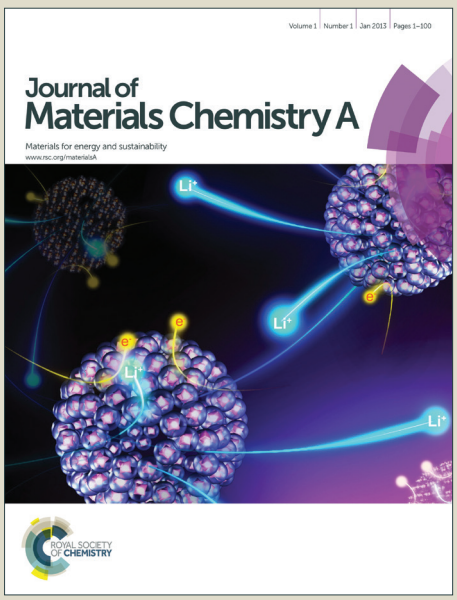

ROYAL SOCIETY OF CHEMISTRY

www.rsc.org/materialsA

High performance dielectric composites by latex compounding of graphene oxide-encapsulated carbon nanosphere hybrids with XNBR

Ming Tian[1, 2], Qin Ma[1], Xiaolin Li[1, 2], Liqun Zhang[1, 2], Toshio Nishi[3], and Nanying Ning[1, 2*]

1. State Key Lab of Organic-Inorganic Composites, Beijing University of Chemical Technology, Beijing 100029, China;
2. Key Laboratory of Carbon Fiber and Functional Polymers, Ministry of Education, Beijing University of Chemical Technology, Beijing 100029, China;
3. Department of Applied Physics, The University of Tokyo, Hongo, Bunkyo-ku, Tokyo, Japan.

Abstract: A novel dielectric composite with high dielectric constant (*k*), low dielectric loss, low elastic modulus and large actuated strain at a low electric filed was prepared by a simple, low-cost and efficient method. The graphene oxide nanosheets (GO)-encapsulated carbon nanosphere (GO@CNS) hybrids were fabricated for the first time via π-π interaction and hydrogen bonding interaction by simply mixing the CNS and GO suspension. The assembly of GO@CNS hybrids around rubber latex particles was realized by hydrogen bonding interaction between carboxylated nitrile rubber (XNBR) and GO@CNS hybrids during latex compounding. The thermally reduced GO (RGO)@CNS/XNBR composites were then obtained from GO@CNS/XNBR by vulcanization and in situ thermal reduction, resulting in the formation of a segregated filler network. The results showed that *k* at 10^3 Hz obviously increased from 28 for pure XNBR to 400 for the composite with 0.75 vol. % of the hybrids because of the formation of segregated filler network and the increased interfacial polarization ability of the hybrids after in situ partially thermal reduction. Meanwhile, the composite with 0.75 vol. % of the hybrids retained low conductivity (10^{-7} S/m), resulting in the low dielectric

*Corresponding author. E-mail: ningny@mail.buct.edu.cn (N. Ning).

loss (<0.65 at 10^3 Hz). In addition, the elastic modulus only mildly increased with the addition of 0.75 vol. % of the hybrids, retaining the good flexibility of the composites. More interestingly, the actuated strain at 7 kV/mm obviously increased from 2.69% for pure XNBR to 5.68% for the composite with 0.5 vol. % of RGO@CNS, and the actuated strain at a lower electric field (2 kV/mm) largely increased from 0.23% for pure XNBR to 3.06% for the composite with 0.75 vol. % of RGO@CNS, much higher than that of other dielectric elastomers reported in previous studies, facilitating the application of dielectric elastomer in biological and medical fields, where a low electric field is required.

Keywords: graphene oxide-encapsulated carbon nanosphere (GO@CNS) hybrids, dielectric properties, latex compounding, in situ thermal reduction

1. Introduction

Dielectric elastomers (DEs) can give rise to surprisingly large deformations by applying an electric field, thus have been receiving much attention in the past two decades.[1-3] By virtue of low modulus, large strain, fast response, lightweight, reliability, high energy density, and high electromechanical coupling efficiency,[4-6] DEs have found many applications in industry such as artificial muscles, sensors, micro air vehicles, flat-panel speakers, micro-robotics and responsive prosthetics.[7-11] A key limitation for the practical application of dielectric elastomer actuators (DEAs) is the requirement of high operating electric field (>100 kV/mm),[7, 12, 13] which could be harmful to humans and damage equipment, particularly in biological and medical fields.[12-14] Getting a large actuated strain at a low electric field is the biggest challenge for DEAs.

To obtain a DE with high actuated strain at a low electric field, a high electromechanical

sensitivity (β) is required, which is defined as the ratio of the dielectric constant (k) to the elastic modulus (Y) (β= k /Y). Accordingly, a substantial increase in dielectric constant and a substantial decrease in elastic modulus is a reasonable solution.[15-17] A disadvantage for DEs is that the k is quite low such as polyurethane elastomer (k = 7.0),[18]acrylic rubber (k = 4.8)[6] and silicone elastomer (k = 2.8).[6] Thus, a key issue is to increase the k of DEs while retaining other excellent performance such as low dielectric loss, and low elastic modulus. The most commonly used approach to increase the k of a polymer is to introduce high k ceramic powders such as TiO_2[19] and $BaTiO_3$[20] into the elastomer matrix. In this case, a high content (up to 50 vol. %) of ceramics is usually required to obtain a high k, resulting in high elastic modulus, low flexibility, and poor processability, thus largely limiting the applications of DEs. Another approach is to add conductive fillers such as carbon nanotubes (CNTs) or graphene sheets into the elastomer matrix to prepare percolative composites.[21-24] Compared with CNTs, graphene sheets are usually synthesized from natural graphite, which are abundant, cheap and easily available. More importantly, graphene sheets have a larger aspect ratio, and thus have been considered to be an ideal candidate as high k filler. [21]

Many studies have been focused on improving the dielectric properties of polymer by introducing graphene oxide nanosheets (GO) into polymer matrix.[24, 25] However, the increase in k of these polymers by adding GO is far less than expected.[24, 25] The major reasons include the poor dispersion of GO in matrix, the restacking of GO during sample preparation process because of π-π stacking and hydrophobic interactions, and/or weak interfacial adhesion between GO and polymer matrixes.[21, 23] The organic functionalization of GO provides a promising way to obtain a good dispersion of GO in the polymer matrix and a strong interfacial adhesion between GO and the matrix.[26-28] In addition, the encapsulation of GO on

the surface of silica, metal oxide particles, carbon nanotubes or carbon nanosphere (CNS) is an efficient method to prevent GO from self-agglomerating, as reported in previous studies.[29-33] Of these particles, CNS has several advantages. First, CNS has graphite structure, and thus GO encapsulated CNS hybrid could be prepared simply via π-π interaction, as reported in graphene/fullerene system in previous study.[34] Second, both CNS and reduced GO can be used as good dielectric fillers because of similar graphite structure.[35] More importantly, CNS with spherical shape could have less effect on the increase in elastic modulus of the composites at the same filler content comparing with fibrous CNTs and layered GO.

Herein, we first prepared GO encapsulated CNS hybrids (GO@CNS) via π-π interaction and hydrogen bonding interaction by simply mixing the CNS and GO suspension without using any modifier/surfactant. Carboxylated nitrile rubber (XNBR), which contains a large amount of strong polar groups (carboxyl groups and cyano groups), has a high dielectric constant (>10), good mechanical strength, good oil and solvent resistance, and thus XNBR latex was used as the rubber matrix for the directionally self-assembly with GO@CNS hybrid. The homogeneous compounded latex of GO@CNS/XNBR was obtained through ultrasonically-assisted latex compounding. The directionally distributing of GO@CNS at the boundary between rubber latex particles was obtained by the hydrogen bonding between carboxyl groups of XNBR and oxygen-containing groups (hydroxyl, carboxyl and carbonyl groups) of GO, resulting in the formation of a segregated GO@CNS network at a low percolation threshold. Finally, GO@CNS in the composites was partially thermally reduced at moderate temperature (180 ºC). Our goal is to prepare dielectric composites with high *k*, low dielectric loss, low elastic modulus and large actuated strain at a low electric field for the wide application of DEs and to clarify the relationship between microstructure and dielectric

properties. To the best of our knowledge, dielectric composites with a segregated network structure have not been reported yet.

2. Experimental

2.1. Materials

Natural graphite flakes with a mean size of 18 μm were supplied by Huadong Graphite Factory (China). Carbon nanosphere with an average diameter of 100 nm was synthesized by us. A commercially available carboxylic acrylonitrile butadiene rubber (XNBR) (Nipol 1571H, solid content 40 wt. %, cyano group content 35 wt. %) was supplied by Zeon Corporation (Japan). Dicumyl peroxide (DCP) was used as the crosslink agent of XNBR. Potassium permanganate ($KMnO_4$, 99.5%), sulfuric acid (H_2SO_4, 98%), sodium nitrate ($NaNO_3$, 99.0%), hydrogen peroxide (H_2O_2, 30%), hydrochloric acid (HCl, 37%), and methanol (CH_3OH, 99.5%), which were all used for the preparation of graphite oxide, were supplied by Beijing Chemical Reagents Co., Ltd. (China).

2.2. Preparation of graphene oxide-encapsulated carbon nanosphere (GO@CNS) hybrids

Graphite oxide was prepared from natural graphite by Hummers method.[36] The product was vacuum-filtered and washed with 1:10 HCl aqueous solution (1 L) to remove metal ions followed by 1 L of deionized water to remove the acid, and then dried in a vacuum oven at 60 °C for 24 h.[37]

The as-prepared graphite oxide was then dispersed in aqueous solution (1 mg/mL) and exfoliated via ultrasonication for 1 h by using a GA 98-ⅢⅠultrasonic cell disruptor (Shangjia Biological Technology, China) with a power of 1000 W to form a uniform colloidal suspension of graphene oxide nanosheets. The exfoliated graphene oxide aqueous solution was then centrifuged at 8000 rpm for 10 min to remove the non-exfoliated graphite oxide particles and other impurities.

The CNS were purified by centrifugation, washing and dispersing in water and in alcohol, and then dried at 80 ºC for more than 4 h before use, as conducted in the previous study.[38] The homogeneous suspension of pristine CNS in deionized water was obtained via ultrasonication for 1h. In a typical process, the GO@CNS hybrid was simply fabricated by mixing the neutral aqueous suspension of CNS and GO solution. 400 mL CNS suspension (0.25 mg/mL) was added into 400 mL aqueous GO solution (0.125 mg/mL) under mechanical stirring for 3 h at room temperature. The initial mass ratio of CNS and GO is 2. When the stirring was stopped, the sediment solid (GO@CNS) was filtered by using a membrane filter, and washed with deionized water for three times to remove the unbound GO and other impurities,[29, 39, 40] and then dried by lyophilization.

2.3. Preparation of XNBR composites with latex compounding

The preparation of RGO@CNS/XNBR composites is schematically illustrated in Scheme 1. First, the GO@CNS hybrids with the content ranging from 0.0 to 0.75 vol. % were dispersed in aqueous solvent by ultrasonic treatment (Scheme 1a). Meanwhile, 0.02 g of crosslink agent DCP was dispersed in 10 g of XNBR latex (4 g of XNBR and 6 g of water) by ultrasonication for 2 h. Then, the uniform GO@CNS suspension was mixed with XNBR latex under stirring for 12 h. The GO@CNS/XNBR compounded latex was first concentrated with a spin flash drying apparatus (Re 3000, Shanghai Yarong, China) under reduced pressure at 50 °C, during which the GO@CNS hybrids were self-assembly on the surface of latex particles, due to the strong hydrogen bond interaction between oxygen-containing functional groups (hydroxyl, carboxyl and carbonyl groups) of GO shells and the carbonxyl groups of XNBR matrix (Scheme 1b). The spin flash drying technique helped to get rid of solvent quickly, and thus can effectively promote the well distribution of GO@CNS in the rubber matrix. The

coagulated rubber mixture was completely dried in a vacuum at 60 ºC for 24 h and the GO@CNS/XNBR composites were obtained by vulcanization of the dried rubber mixture at the pressure of 2 MPa at 170 ºC for 20 min. The RGO@CNS/XNBR composites were obtained by in situ thermal reduction of GO@CNS/XNBR composites at the pressure of 3 MPa at 180 ºC for 2 h (Scheme 1c). It should be noted that the RGO content is actually only 0.25 vol. % for the composite with 0.75 vol. % of RGO@CNS because the mass ratio of CNS and GO is 2.

For comparison purpose, CNS/XNBR composites with 0.0-0.75 vol. % of CNS and GO/XNBR composites with 0.0-0.75 vol. % of GO were also prepared at the same condition as that of GO@CNS/XNBR composites. Because of the lack of strong interfacial adhesion effect between CNS and XNBR, CNS could not be dispersed well in the rubber matrix (Scheme 1d).

2.4. Characterization

Fourier transform infrared spectra (FTIR) were conducted by using a Bruker Tensor 27 spectrometer. All the spectra were obtained at a resolution of 4 cm^{-1} in the wave number range of 400 to 4000 cm^{-1}.

The morphology and microstructure of CNS, GO and GO@CNS were investigated by scanning electron microscope (SEM, S-4800, Hitachi Co. Japan), high resolution transmission electron microscope (HRTEM, JEM-3010, Hitachi, Japan), X-Ray Diffraction (XRD, 2500VB2+PC, Rigaku Co., Japan) and UV-vis absorption spectra (UV-3600, Shimadzu, Japan). GO and GO@CNS samples for HRTEM observation were prepared by suspending graphite oxide and GO@CNS in water at the concentration of 0.005 mg/mL under ultrasonication for 30 min, dropping the GO and GO@CNS suspension on micro grids, and

then drying in a vacuum oven, respectively .

Atomic force microscopy (AFM, Nano Scope Analysis, and Bruker, Germany) was used to study the thickness of graphene oxide nanosheets by using the tapping mode. The sample for AFM observation was prepared by suspending graphite oxide in water at the concentration of 0.0025 mg/mL under ultrasonication for 30 min, dropping the suspension on a SiO_2/Si wafer, and drying in a vacuum oven.

An ESCALAB250 X-ray photoelectron spectroscopy (XPS) purchased from Thermo Fisher Scientific Company (American) was used to study the chemical compositions of GO, CNS, GO@CNS and RGO@CNS prepared by thermal reduction of GO@CNS at 180 ºC for 2 h in vacuum oven.

Thermal gravity analysis (TGA) was carried out ranging from 30 ºC to 800 ºC at a heating rate of 10 ºC min^{-1} with a Mettler Toledo TGA1100SF (Switzerland).

The composite samples observed in TEM (Tecnai G^2 20, FEI Co. Hong Kong) examination were cryogenically cut with a glass knife by a Reichert-Jung Ultracut microtome (Leica Camera AG, Germany) and then collected on 400-mesh copper grids.

The volume resistivity (ρ_v) of GO@CNS/XNBR composites was measured by high resistance meter (EST121, Beijing Huajinghui technology co., LTD, China). ρ_v is calculated as follows: $\rho_v = 4L/(R_V \times \pi \times d^2)$, where L is the thickness of the specimen, R_V is the volume resistance, and d is the diameter of the electrode. The conductivity is the reciprocal of volume resistivity.

The dielectric properties of the samples were measured by an impedance analyzer (E4980A, Agilent, U.S.A.) over the frequency range of 20 to 10^6 Hz under a voltage of 220 V at room temperature.

The elastic modulus of pure XNBR and XNBR composites were obtained by calculating the slopes of the stress-strain curves at the strain of 5%, which were obtained by using a tensile apparatus (CMT4104, Shenzhen SANS Testing Machine Co., Ltd., China) at a strain rate of 50 mm/min.

The cyclic stretching stress-strain curves of pure XNBR and XNBR composites were obtained by using a tensile apparatus (CMT4104, Shenzhen SANS Testing Machine Co., Ltd., China) at a strain rate of 5 mm/min, and the largest strain was controlled at 5%. The hysteresis loss of pure XNBR and XNBR composites at 5% of strain were calculated by the ratio of the area of the stress-strain curves and the area of the loading curves below.

The samples for actuated strain tests had a thickness of about 0.5 mm and a diameter of 5 cm, and compliant graphite electrodes with a diameter of 11 mm were applied to each side of the dielectric elastomer films. As it was difficult to accurately measure the change in thickness, we instead measured the change in planar area S_p to evaluate the thickness actuated strain S_z. Based on the law of volume constancy, we can conclude that

$$(1 + S_z)(1 + S_p) = 1 \quad (1)$$

Rearrangement of equation (1) gives an expression for the planar strain:

$$S_p = \frac{1}{1 + S_z} - 1 \quad (2)$$

According to equation (2), the planar strain increases with increasing thickness strain because the thickness strain is negative. Actuated strain tests were performed by using circular membrane actuators, which the dielectric elastomer films were laid flat between two circular frames. Voltages from 0 kV/mm were loaded on the electrode area to obtain planar strain until electric breakdown occurred. During actuation, video images of the biaxial extension of the electrode area film were captured by a camera (Canon Ixus 80, Japan) fitted with a wide-angle lens, and the relative change in planar area was determined by analyzing the captured video

images with Adobe Photoshop graphics editing software. The planar strain can be calculated according to $S_P = (A - A_0) / A_0 \times 100$, where A is the actuated planar area and A_0 is the original area.[41]

Every experimental data of dielectric properties, mechanical properties and electromechanical strain presented in our study was the average of the results obtained from at least three samples under the same conditions.

3. Results and discussion

3.1. Self-assembly of GO and CNS

There exist some hydroxyl groups on the surface of CNS, as demonstrated by the FTIR spectrum of CNS shown in Fig.S1a. There exist many oxygen-containing groups such as hydroxyl groups (3434, 1400 cm^{-1}), carbonyl groups (1720 cm^{-1}), and epoxy groups (1043 cm^{-1}) on GO, as demonstrated by the FTIR spectrum of GO shown in Fig.S1a. GO exhibits sheet structure with a large aspect ratio, as shown in the HRTEM image of Fig.S1b. The thickness of three layers of GO sheets is about 4 nm, indicating that the thickness of single layer of GO sheets is about 1.3 nm, as shown in Fig.S1c. The AFM image of GO (Fig.S1d) also shows the sheet structure of GO with lateral dimensions of several micrometers and an average thickness of about 1.3 nm, which is consistent with the TEM results. The ultrathin GO facilitates the preparation of GO@CNS hybrids.

The direct evidence for the self-assembly of GO on CNS is shown in Fig. 1. Pristine CNS are generally self-aggregated into spherical bodies (see Fig. 1a) because of the presence of reactive dangling bonds on their surface, providing them with a high surface reactivity, as reported in previous study.[35] Compared with pristine CNS particles with smooth surface, the surfaces of GO@CNS hybrids are intimately covered by ultrathin GO films as shown in Fig.

1b-c. The creases and roughened textures are associated with the presence of flexible and ultrathin GO.[29] The typical HRTEM image of GO@CNS hybrid (see Fig. 1d-f) also confirms that the flexible and ultrathin GO have been encapsulated on CNS, with the thickness of GO shells about 3 nm. The core-shell structure of GO@CNS hybrid prevents CNS from self-aggregating and stops restacking of GO. Table S1 shows the XPS results of chemical compositions of GO, CNS, GO@CNS and RGO@CNS. An increase in oxygen content from 5.61% of CNS to 16.44% of GO@CNS suggests the encapsulation of GO on CNS.

Fig.S2 shows the XRD patterns of CNS, GO and GO@CNS hybrids. Both the characteristic diffraction peak ($2\theta = 11.3°$) of GO and the broad characteristic diffraction peak ($2\theta = 25°$) of CNS are observed on the pattern of GO@CNS hybrid, again indicating the self-assembly of GO on CNS. In addition, the intensity of the characteristic peak at 11.3° for pristine GO is sharply reduced for GO@CNS hybrid, indicating that the restacking of GO is inhibited by CNS.

The mechanism for the encapsulating of GO on CNS is schematically represented in Fig. 2a. The encapsulating of GO on CNS was realized via the hydrogen bonding (H-bonding) interaction between oxygen-containing groups of GO and the hydroxyl groups of CNS as well as the π-π interaction between GO and CNS. The H-bonding interaction between oxygen-containing groups of GO and hydroxyl groups has been demonstrated in previous studies.[42-44] The FTIR spectra of CNS, GO and GO@CNS hybrid were used to understand the H-bonding interaction between CNS and GO, as shown in Fig. S1a. The absorption peak of hydroxyl group (–OH) centered at 3436 cm^{-1} for CNS shifts to 3444 cm^{-1} for the GO@CNS hybrid (see Fig.S1a), suggesting the formation of H-bonding between the hydroxyl groups (–OH) of CNS and the carboxylic groups (–COOH), carbonyl groups (C=O) and hydroxyl

groups (–OH) of the GO sheets. The π-π interaction between GO and CNS was demonstrated by UV-vis absorption spectra, as shown in Fig. 2b. A broad absorption peak is observed for pristine CNS, whereas an absorption peak centered at 228 nm is observed for pristine GO, ascribed to the π-π transitions of aromatic C-C bonds.[31] The absorption peak at 228 nm of pristine GO shifts to 237 nm on the spectrum of GO@CNS hybrids, demonstrating the π-π stacking interactions of the multiple aromatic regions between GO and CNS.[31] It is indicated for the first time that directly self-assembling of GO on CNS (GO@CNS hybrids) can be realized via hydrogen bonding interaction and π-π interaction by simply mixing the CNS and GO suspension without using any modifier/surfactant.

3.2. Microstructure of GO@CNS*/XNBR composites*

GO@CNS/XNBR composites were prepared via self-assembly of GO@CNS hybrids and XNBR latex, as described in section 2.3. The TEM image of the as-prepared GO@CNS/XNBR composites with 0.75 vol. % of hybrids is shown in Fig. 3a. As expected, a large number of GO@CNS hybrids are uniformly distributed around the surface of XNBR particles and are connected with one another to form a segregated network structure. This is ascribed to the hydrogen bonding interaction between oxygen-containing groups of GO and carboxyl groups of XNBR latex, as demonstrated in the previous work.[45] For comparison purpose, the TEM image of pristine CNS/XNBR composites with the same filler content is observed, as shown in Fig. 3b. We can observe severe agglomeration of CNS in XNBR matrix, ascribed to the high surface reactivity of CNS, as reported in the previous study.[35]

3.3. In situ thermal reduction of GO@CNS/XNBR composites

Many studies have demonstrated that the increase in *k* is far less than expected by using GO as the dielectric filler because of the severe disruption of graphite structure of GO.[22, 25]

Therefore, the reduction of GO@CNS/XNBR composites is required to increase the interfacial polarization ability of GO@CNS. Thus, in this study, the in situ thermal reduction of GO@CNS/XNBR composites was conducted at 180 ºC for 2 h under vacuum because of the following advantages. First, the directional distribution of GO@CNS around XNBR latex particles and the segregated network structure can be retained during in situ thermal reduction at 180 ºC. Second, the method is simple and efficient for the partial reduction of GO shells of GO@CNS hybrids.[25, 46, 47]

Thermal reduction of pure GO@CNS hybrids was conducted under the same condition to evaluate the reduction degree of GO shells. The degree of reduction was characterized by using XPS and TGA, and the results are shown in Table S1 and Fig. 4. The oxygen content obviously decreases from 16.44% for GO@CNS to 12.23% for RGO@CNS as shown in Table S1, suggesting the partial reduction of GO shells. Fig. 4a shows the XPS C1s core-level spectra of pure GO@CNS hybrids. We can observe four characteristic peaks corresponding to carbon atoms in different functional groups: C–C (unoxidized graphite carbon skeleton) at 284.9 eV, C–O (hydroxyl and epoxy group) at 286.7 eV, C=O (carbonyl) groups at 288.1 eV and COOH (carboxyl and ester) groups at 289.1 eV. The presence of the same peaks in Fig. 4b suggests that there are still some oxygen-containing groups in RGO@CNS hybrids. But these peaks corresponding to the oxygen-containing groups in the spectrum of RGO@CNS are weakened, especially that of C=O (carbonyl), indicating that GO shells have been partially reduced during thermal reduction at 180 °C.

The mass loss of pure GO, CNS, GO@CNS and RGO@CNS was measured at a heating rate of 10 ºC/min in nitrogen atmosphere, as shown in Fig. 4c. The mass loss of CNS at 800 °C is less than 6%, suggesting the good thermal stability of CNS. The mass loss below

100 °C of GO and GO@CNS is due to the removal of adsorbed water. The maximum rate of mass loss, corresponding to the loss of most of the oxygen-containing groups, occurs at 170-230 °C for both GO and GO@CNS, again indicating the self-assembly of GO on CNS. Compared with GO@CNS, the mass loss of RGO@CNS at 170-230 °C is largely decreased, again indicating the reduction of GO shells of GO@CNS hybrids. Compared with CNS, the mass loss of RGO@CNS continues with the further increase in temperature because of the remained oxygen-containing groups caused by the partial reduction of GO shells during thermal reduction at 180 °C.

The reduction of GO@CNS in XNBR matrix is also demonstrated by the change in electrical conductivity (σ) of composites after in situ thermal reduction, as shown in Fig. 4d. We can see that the electrical conductivity increases obviously with the increase in the content of GO@CNS. It should be noted that the pristine CNS has good conductivity,[48] whereas GO@CNS hybrid is electrically insulated because of the insulated GO shells.[49] The electrical conductivity of the same composite is increased after thermal reduction, indicating that GO shells of the hybrids are partially reduced in XNBR matrix. In addition, the electrical conductivity of all the composites is still less than 10^{-6} S/m, much lower than that of other conductive filler/elastomer composites, as summarized in Table S2 (see the supporting information).

3.4. Electromechanical properties of RGO@CNS/XNBR composites

The dielectric properties of pure XNBR and RGO@CNS/XNBR composites measured at room temperature are shown in Fig. 5 and Fig. 6. The frequency response of the *k* of the composites with various contents of RGO@CNS is shown in Fig. 5a. As expected, the *k* of all the RGO@CNS/XNBR composites is largely decreased with the increase in frequency,

suggesting a strong frequency dependence of *k* of all the composites. The strong frequency dependence of *k* is ascribed to the interfacial polarization effect (also named as Maxwell-Wagner-Sillars (MWS) effect) of RGO@CNS on XNBR molecules caused by the accumulation of many free charges at the internal interfaces between RGO@CNS and XNBR.[50] It has enough time to accumulate charge at the interfaces between RGO@CNS and rubber matrix at low frequency, resulting in the high *k* of the composites. However, the interfacial polarization cannot catch up with the change in electrical field frequency at high frequency, leading to the large decrease in *k* at high frequency.[51]

Interestingly, a sharp increase in *k* is observed with the presence of 0.25 vol. % of RGO@CNS, suggesting that a very low percolation threshold is obtained by directionally distributing of RGO@CNS around XNBR rubber particles, as shown in Fig. 5a. The *k* of the composites are further sharply increased with the increase in the content of RGO@CNS because of the formation of a more completed network structure, as demonstrated in section 3.2. The detailed values of *k* of pure XNBR and RGO@CNS/XNBR composites at 10^3 Hz are summarized in Fig. 5b. We can observe that *k* at 10^3 Hz obviously increases from 28 for pure XNBR to 400 for the composite with 0.75 vol. % of RGO@CNS.

The *k* of GO@CNS/XNBR composites at 10^3 Hz before thermal reduction was also studied, and the results are summarized in Fig. 5b in order to demonstrate the effect of in situ thermal reduction of GO@CNS on the increase in *k*. We can observe that *k* obviously increases with the increase in the content of GO@CNS, indicating that GO@CNS still has interfacial polarization ability on XNBR to increase the *k* as a dielectric filler network structure formed in the composites. After thermal reduction, *k* is sharply increased at the same filler content. For example, *k* is increased from 113 to 400 for the composite with 0.75 vol. % of GO after in

situ thermal reduction, demonstrating the large increase in interfacial polarization ability of RGO@CNS by using in situ thermal reduction at 180 °C.

CNS core as a kind of dielectric filler could also play a role in the increase in *k*. Thus, the dielectric properties of CNS/XNBR composites were investigated, and the results are shown in Fig. S3. We can observe that although the *k* is increased with the increase in the content of CNS, the increase of *k* is much less than that of RGO@CNS/XNBR composites at the same filler content. The maximum of *k* at 10^3 Hz of CNS/XNBR composites is lower than 60, indicating that the main contribution for the large increase in *k* of RGO@CNS composites is from RGO shells.

The dielectric loss of pure XNBR, GO@CNS/XNBR and RGO@CNS/XNBR composites are shown in Fig. 6. We can observe that the dielectric loss of all the composites keeps at a relatively low level (<0.65 at 10^3 Hz), much lower than that of many other conductive filler/polymer dielectric composites, as summarized in Table S2 (see the support information). The relatively low loss is mainly attributed to the low DC conductance of RGO@CNS caused by the partial reduction of GO shells by in situ thermal reduction at 180 ºC, as demonstrated by the relatively low electrical conductivity of all the composites (see section 3.3).[21]

The elastic modulus of pure XNBR and RGO@CNS/XNBR composites are summarized in Table 1. We can observe that the elastic modulus is mildly increased from 1.7 MPa for pure XNBR to 2.1 MPa and 3.2 MPa for the composites with 0.25 vol. % and 0.75 vol. % of RGO@CNS, respectively. The large increase in the *k* and the mild increase in the elastic modulus of XNBR composites by adding RGO@CNS lead to the large increase in the electromechanical sensitivity (β) of XNBR, as summarized in Table 1. We can observe that β at 10^3 Hz sharply increases from 14.7 MPa^{-1} for pure XNBR to 21.4 MPa^{-1} and 125 MPa^{-1} for

the composites with 0.25 vol. % and 0.75 vol. % of RGO@CNS, respectively. Comparing with pure XNBR, β of XNBR increases by 46% and 750 % by adding 0.25 vol. % and 0.75 vol. % of RGO@CNS, respectively. The large increase in β leads to the large increase in actuated strain of RGO@CNS/XNBR composites at a low electric field (see below).

Fig. 7 shows the actuated strains of pure XNBR and RGO@CNS/XNBR composites as a function of electric field. The actuated strain of all the samples obviously increases with the increase in electric field because it has a quadratic relationship with the applied electric field. Although the maximum actuated strain of the composites is slightly higher or even lower than that of pure XNBR and the breakdown strength of XNBR obviously decreases with the increase in RGO@CNS content, the actuated strain of the composites at very low electric field is much higher than that of pure XNBR, as summarized in Table 1. For example, the actuated strain at 7 kV/mm obviously increases from 2.69% for pure XNBR to 5.68% for the composite with 0.5 vol. % of RGO@CNS. More interestingly, the actuated strain at 2 kV/mm obviously increases from 0.23% for pure XNBR to 3.06% for the composite with 0.75 vol. % of RGO@CNS, 13-fold increase in the actuated strain. To our best knowledge, the actuated strain at 2 kV/mm of the composite with 0.75 vol. % of RGO@CNS, and the actuated strain at 7 kV/mm of the composite with 0.5 vol. % of RGO@CNS are much larger than other DE systems at the same electric field reported in many previous studies, as summarized in Table 2.[12, 41, 52-58] Here, it should be noted that the actuated strain tests were performed by using circular membrane actuators without prestrain. The large increase in actuated strain at very low electric field is ascribed to the large increase in β caused by the large increase in *k*. The dielectric composites are still safe when the operated electric voltage is lower than the breakdown voltage, as reported in the reference.[59] The large actuated strain at a low electric

field facilitates the application of DE materials in biological and medical fields, where a low electric field is required for safety of human bodies.

The cyclic stress-strain curves of pure XNBR and the RGO@CNS/XNBR composites with 0.25 vol. % and 0.75 vol. % of RGO@CNS and the corresponding hysteresis loss at 5% of strain are shown in Fig. 8. We can observe that both the stress at certain strain and the Young's modulus (the slope of the curve) increase with the increase in the content of RGO@CNS, indicating the reinforcement effect of RGO@CNS on XNBR matrix, as shown in Fig. 8a. The hysteresis loss of pure XNBR at 5% of strain is up to 26.2% because of the high content of polarized groups (carboxyl groups and acrylonitrile groups) of XNBR (see section 2.1). The hysteresis loss at 5% of strain is only slightly increased with the addition of 0.25 vol. % and 0.75 vol. % of RGO@CNS (see Fig. 8b), indicating that the addition of 0.25 vol. % or 0.75 vol. % of RGO@CNS has almost no effect on the hysteresis loss of XNBR matrix.

3.5. Advantages of using RGO@CNS hybrids as the dielectric filler

The advantages of using RGO@CNS hybrids as the dielectric filler are three folds. First, the self-assembly of GO on CNS prevents the restacking of GO sheets. Second, the self-assembly of GO on CNS makes it much easier to form a dielectric filler network at a low GO content because of the filling effect of CNS. The third advantage is the lower elastic modulus of RGO@CNS/XNBR composite than that of RGO/XNBR composite at the same filler content because of the spherical shape of RGO@CNS hybrids (see Fig. 9a), a big advantage for the preparation of high performance DE. In addition, at the same content of RGO (0.25 vol. %), the elastic modulus of the RGO@CNS/XNBR composite with 0.75 vol. % of RGO@CNS is almost the same as that of RGO/XNBR composite with 0.25 vol. %

of RGO. Fig. 9b compares the *k* and β of XNBR composites with 0.75 vol. % of RGO@CNS (containing 0.25 vol. % of RGO) and 0.25 vol. % of RGO at 10^3 Hz. We can observe that the *k* of the RGO@CNS/XNBR composites (*k* =400) is much higher than that of RGO/XNBR composites (*k* =143) at the same RGO content (0.25 vol. %). As a result, the β of the RGO@CNS/XNBR composites (β =125.0) is much higher than that of RGO/XNBR composites (β =46.2) at the same RGO content. Fig. 9c compares the actuated strain of XNBR composites with 0.75 vol. % of RGO@CNS and the composite with 0.25 vol. % of RGO. Although the breakdown strength of the composite with 0.75 vol. % of RGO@CNS is lower than that of the composite with 0.25 vol. % of RGO, the actuated stain (3.06%) of the composite with 0.75 vol. % of RGO@CNS at the same electric field (2 kV/mm) is much higher than that (0.36%) of the composite with 0.25 vol. % of RGO at the same RGO content.

4. Conclusions

We developed a facile, simple and efficient method to fabricate a novel dielectric composite with high *k*, low dielectric loss, low elastic modulus and large actuated strain at a low electric field. The core-shell structured GO@CNS hybrid was fabricated for the first time without using any surfactant/modifier, and then the RGO@CNS/XNBR composites with a segregated filler network was prepared by blending XNBR latex with GO@CNS aqueous suspension and followed by vulcanization and in situ thermal reduction, where the hybrids were directionally distributed around rubber latex particles by hydrogen bonding interaction between XNBR and GO. The RGO@CNS/XNBR composites exhibited high dielectric constant, low electrical conductivity, and thus low dielectric loss because of the partial thermal reduction of GO shells. Because of the advantages of using RGO@CNS hybrids as the dielectric filler instead of RGO, the *k* of RGO@CNS/XNBR composite (400 at 10^3 Hz) was much higher than that of

RGO/XNBR composite (134 at 10^3 Hz) at the same RGO content (0.25 vol. %), whereas their elastic modulus were almost the same. As a result, at the same electric field, the actuated strain of RGO@CNS/XNBR composite was much higher than that of RGO/XNBR composite at the same RGO content (0.25 vol. %). More importantly, the large *k* and the low elastic modulus of the RGO@CNS/XNBR composites resulted in the achievement of large actuated strain (3.06%) at a very low electric field (2 kV/mm), much higher than that reported in other studies, facilitating the application of dielectric elastomer in biological and medical fields, where a low electric field is required. In addition, the hysteresis loss at 5% of strain of RGO@CNS/XNBR composite was almost the same as that of pure XNBR.

Acknowledgements

We would like to express our sincere thanks to the National Natural Science Foundation of China (Grant No.51173007, 51103090 and 51221002) for financial support.

References

1. Y. Rao and C. Wong, *J. Appl. Polym. Sci.*, 2004, **92**, 2228-2231.
2. Y. Song, Y. Shen, H. Liu, Y. Lin, M. Li and C.-W. Nan, *J. Mater. Chem.*, 2012, **22**, 16491-16498.
3. H. Stoyanov, M. Kollosche, S. Risse, D. N. McCarthy and G. Kofod, *Soft Matter*, 2011, **7**, 194-202.
4. G. Ouyang, K. Wang and X. Chen, *J. Micromech. Micoeng.*, 2012, **22**, 074002.
5. Y. Jang and T. Hirai, *Soft Matter*, 2011, **7**, 10818-10823.
6. R. Shankar, T. K. Ghosh and R. J. Spontak, *Soft Matter*, 2007, **3**, 1116-1129.
7. L. Z. Chen, C. H. Liu, C. H. Hu and S. S. Fan, *Appl. Phys. Lett.* , 2008, **92**, 263104.
8. A. Tiwari, A. P. Mishra, S. R. Dhakate, R. Khan and S. K. Shukla, *Mater. Lett.*, 2007,

61, 4587-4590.

9. R. Palakodeti and M. R. Kessler, *Mater. Lett.*, 2006, **60**, 3437-3440.

10. S. M. Ha, W. Yuan, Q. Pei, R. Pelrine and S. Stanford, *Adv. Mater.*, 2006, **18**, 887-891.

11. R. Pelrine, R. Kornbluh, Q. Pei and J. Joseph, *Science*, 2000, **287**, 836-839.

12. F. Carpi, G. Gallone, F. Galantini and D. De Rossi, *Adv. Funct. Mater.*, 2008, **18**, 235-241.

13. C. Huang and Q. Zhang, *Adv. Funct. Mater.*, 2004, **14**, 501-506.

14. M. Molberg, Y. Leterrier, C. J. G. Plummer, C. Walder, C. Löwe, D. M. Opris, F. A. Nüesch, S. Bauer and J.-A. E. Månson, *J. Appl. Phys.*, 2009, **106**, 054112.

15. A. OHalloran, F. OMalley and P. McHugh, *J. Appl. Phys.*, 2008, **104**, 071101-071110.

16. M. Wissler and E. Mazza, *Sensor. Actuat. A-Phys.*, 2007, **138**, 384-393.

17. G. Kofod and P. Somrner-Larsen, in *Electrets, 2005. ISE-12. 2005 12th International Symposium on*, IEEE, 2005, pp. 208-211.

18. K. Wongtimnoi, B. Guiffard, A. Bogner-Van De Moortele, L. Seveyrat, C. Gauthier and J.-Y. Cavaillé, *Compos. Sci. Technol.*, 2011, **71**, 885-892.

19. F. Carpi and D. D. Rossi, *Dielectrics and Electrical Insulation, IEEE Transactions on*, 2005, **12**, 835-843.

20. E. Cherney, *Dielectrics and Electrical Insulation, IEEE Transactions on*, 2005, **12**, 1108-1115.

21. L. J. Romasanta, M. Hernández, M. A. López-Manchado and R. Verdejo, *Nanoscale res. lett.*, 2011, **6**, 1-6.

22. C. Wu, X. Huang, G. Wang, X. Wu, K. Yang, S. Li and P. Jiang, *J. Mater. Chem.*, 2012, **22**, 7010-7019.

23. L. Seveyrat, A. Chalkha, D. Guyomar and L. Lebrun, *J. Appl. Phys.*, 2012, **111**, 104904-104909.

24. Z. Wang, J. K. Nelson, H. Hillborg, S. Zhao and L. S. Schadler, *Adv. Mater.*, 2012, **24**, 3134-3137.

25. H. Tang, G. J. Ehlert, Y. Lin and H. A. Sodano, *Nano letters*, 2012, **12**, 84-90.

26. H. J. Salavagione, G. Martínez and G. Ellis, *Macromol. Rapid. Comm.*, 2011, **32**, 1771-1789.

27. T. Kuilla, S. Bhadra, D. Yao, N. H. Kim, S. Bose and J. H. Lee, *Prog. Polym. Sci.*, 2010, **35**, 1350-1375.

28. D. Chen, H. Feng and J. Li, *Chem. Rev.*, 2012, **112**, 6027-6053.

29. L. Chen, S. Chai, K. Liu, N. Ning, J. Gao, Q. Liu, F. Chen and Q. Fu, *ACS Appl. Mater. Interfaces*, 2012, **4**, 4398-4404.

30. W. Zhou, J. Zhu, C. Cheng, J. Liu, H. Yang, C. Cong, C. Guan, X. Jia, H. J. Fan and Q. Yan, *Energy Environ. Sci.*, 2011, **4**, 4954-4961.

31. C. Zhang, L. Ren, X. Wang and T. Liu, *J. Phys. Chem. C*, 2010, **114**, 11435-11440.

32. X. Dong, G. Xing, M. B. Chan-Park, W. Shi, N. Xiao, J. Wang, Q. Yan, T. C. Sum, W. Huang and P. Chen, *Carbon*, 2011, **49**, 5071-5078.

33. C. X. Guo and C. M. Li, *Energy Environ. Sci.*, 2011, **4**, 4504-4507.

34. D. Wu, F. Zhang, H. Liang and X. Feng, *Chem. Soc. Rev.*, 2012, **41**, 6160-6177.

35. A. Nieto-Márquez, R. Romero, A. Romero and J. L. Valverde, *J. Mater. Chem.*, 2011, **21**, 1664-1672.

36. W. S. Hummers Jr and R. E. Offeman, *J. Am. Chem. Soc.*, 1958, **80**, 1339-1339.

37. C. Wu, X. Huang, X. Wu, L. Xie, K. Yang and P. Jiang, *Nanoscale*, 2013, **5**,

3847-3855.

38. X. Sun and Y. Li, *Angew. Chem. Int. Edit.* 2004, **43**, 597-601.

39. X. Zhang, Y. Huang, Y. Wang, Y. Ma, Z. Liu and Y. Chen, *Carbon*, 2009, **47**, 334-337.

40. F. Luo, L. Chen, N. Ning, K. Wang, F. Chen and Q. Fu, *J. Appl. Polym. Sci.*, 2012, **125**, E348-E357.

41. D. Yang, M. Tian, D. Li, W. Wang, F. Ge and L. Zhang, *J. Mater. Chem. A*, 2013, **1**, 12276-12284.

42. J. Liang, Y. Huang, L. Zhang, Y. Wang, Y. Ma, T. Guo and Y. Chen, *Adv. Funct. Mater.*, 2009, **19**, 2297-2302.

43. H. J. Salavagione, G. Martínez and M. A. Gómez, *J. Mater. Chem.*, 2009, **19**, 5027-5032.

44. X. Yang, X. Zhang, Z. Liu, Y. Ma, Y. Huang and Y. Chen, *J. Phys. Chem. C*, 2008, **112**, 17554-17558.

45. H. Kang, K. Zuo, Z. Wang, L. Zhang, L. Liu and B. Guo, *Compos. Sci. Technol.*, 2014, **92**, 1-8.

46. A. J. Glover, M. Cai, K. R. Overdeep, D. E. Kranbuehl and H. C. Schniepp, *Macromolecules.*, 2011, **44**, 9821-9829.

47. M. Traina and A. Pegoretti, *J. Nanopart. Res.*, 2012, **14**, 1-6.

48. D. Yuan, J. Chen, J. Zeng and S. Tan, *Electrochem. Commun.*, 2008, **10**, 1067-1070.

49. Y. Zhu, M. D. Stoller, W. Cai, A. Velamakanni, R. D. Piner, D. Chen and R. S. Ruoff, *Acs Nano*, 2010, **4**, 1227-1233.

50. X. Huang, P. Jiang and L. Xie, *Appl. Phys. Lett.*, 2009, **95**, 242901-242903.

51. Z. M. Dang, L. Wang, Y. Yin and Q. Zhang, *Adv. Mater.*, 2007, **19**, 852-857.

52. D. M. Opris, M. Molberg, C. Walder, Y. S. Ko, B. Fischer and F. A. Nüesch, *Adv. Funct. Mater.*, 2011, **21**, 3531-3539.

53. D. Yang, L. Zhang, H. Liu, Y. Dong, Y. Yu and M. Tian, *J. Appl. Polym. Sci.*, 2012, **125**, 2196-2201.

54. B. Kussmaul, S. Risse, G. Kofod, R. Waché, M. Wegener, D. N. McCarthy, H. Krüger and R. Gerhard, *Adv. Funct. Mater.*, 2011, **21**, 4589-4594.

55. H. Zhao, D.-R. Wang, J.-W. Zha, J. Zhao and Z.-M. Dang, *J. Mater. Chem. A*, 2013, **1**, 3140-3145.

56. S. Risse, B. Kussmaul, H. Krüger and G. Kofod, *Adv. Funct. Mater.*, 2012, **22**, 3958-3962.

57. C. Huang and Q. M. Zhang, *Adv. Mater.*, 2005, **17**, 1153-1158.

58. D. Yang, M. Tian, H. Kang, Y. Dong, H. Liu, Y. Yu and L. Zhang, *Mater. Lett.*, 2012, **76**, 229-232.

59. F. Carpi, D. De Rossi, R. Kornbluh, R. E. Pelrine and P. Sommer-Larsen, *Dielectric elastomers as electromechanical transducers: Fundamentals, materials, devices, models and applications of an emerging electroactive polymer technology*, Elsevier, 2011.

Table 1. Elastic modulus, dielectric properties and actuated strain of XNBR with different contents of RGO@CNS.

Filler content (vol. %)	**Dielectric constant *k* at 10^3 Hz**	**Dielectric loss tangent at 10^3 Hz**	**Elastic modulus Y (MPa)**	**β= *k*/Y (MPa^{-1})**	**Breakdown strength (kV/mm)**	**Maximal actuated strain (%)**	**Actuated strain at 7 kV/mm (%)**	**Actuated strain at 2 kV/mm (%)**
0	25	0.19	1.7	14.7	14.3	5.12	2.69	0.23
0.1	31	0.27	2.0	15.5	12.5	5.12	2.87	0.39
0.25	45	0.56	2.1	21.4	8.0	5.22	4.93	1.41
0.5	131	0.57	2.3	56.9	7.0	5.68	5.68	1.94
0.75	400	0.63	3.2	125.0	2.0	3.06	/	3.06

Table 2. Summary and comparison of actuation performances of advanced DE composites.

Composites	**Maximum actuated strain (%)**	**Actuated strain at 7 kV/mm (%)**	**Actuated strain at 2 kV/mm (%)**
PHT/PDMS[12]	8.0 (8 kV/mm)	4.6	0.4
PDVB@PANI/PDMS[52]	16.0 (43 kV/mm)	0.06	0.01
PMN/PDMS[53]	8.0 (53 kV/mm)	<1.0	<1.0
Dipoles-PDMS[54]	1.4 (16 kV/mm)	0.4	<0.01
TiO_2-PDMS (plasticized)[55]	18.0 (37 kV/mm)	2.0	<1.0
Allyl-cyano filled silicon[56]	10.0 (48 kV/mm)	1.2	<0.01
$BaTiO_3$-PDA/HNBR[41]	20.0 (45 kV/mm)	<2.0	<2.0
PANI-PolyCuPc/PU[57]	7.0 (23 kV/mm)	0.6	<0.1
polyester elastomer[58]	12.0 (15 kV/mm)	2.0	<1.0
RGO@CNS/XNBR in our study	5.68 (7.0 kV/mm)	5.68	3.06

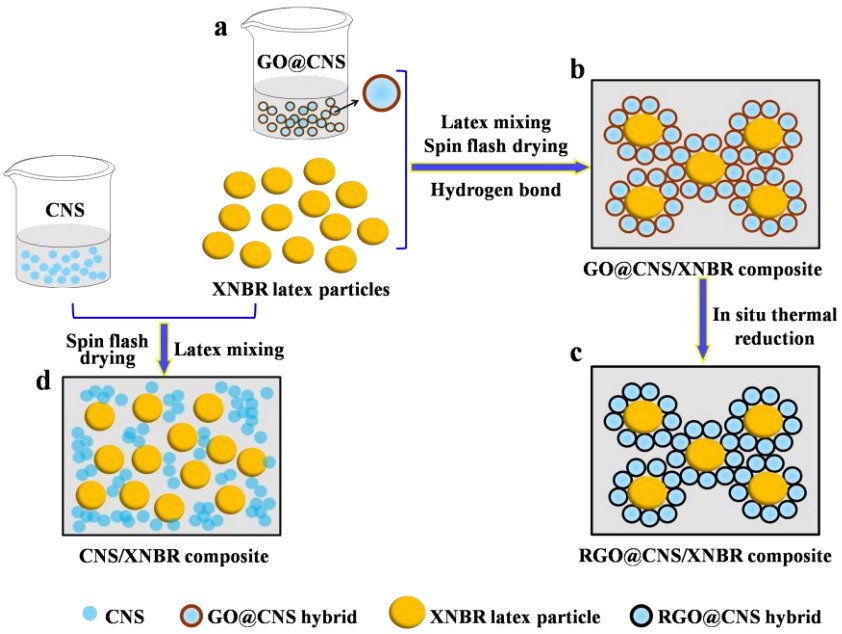

Scheme 1 Schematic representation of the preparation of RGO@CNS/XNBR and CNS/XNBR composite.

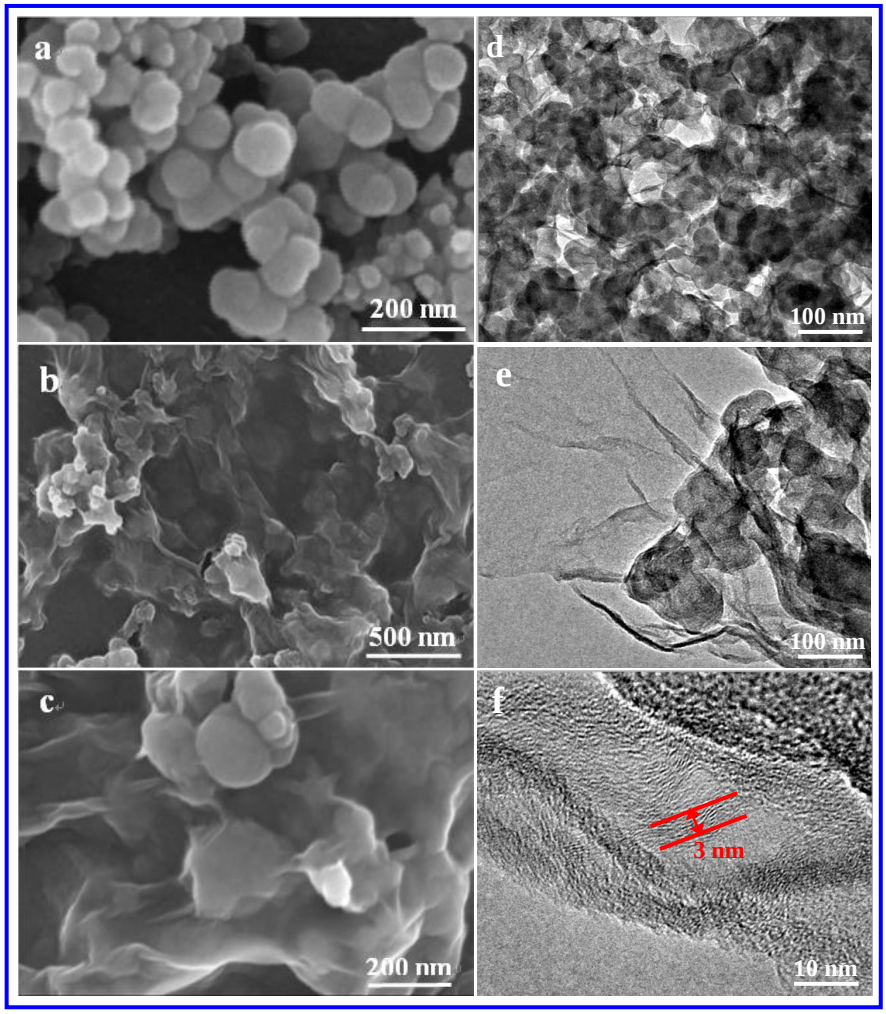

Fig. 1 SEM images of (a) raw CNS and (b, c) GO@CNS hybrids at different magnifications, and (d, e, f) high-resolution TEM (HRTEM) images of GO@CNS hybrids.

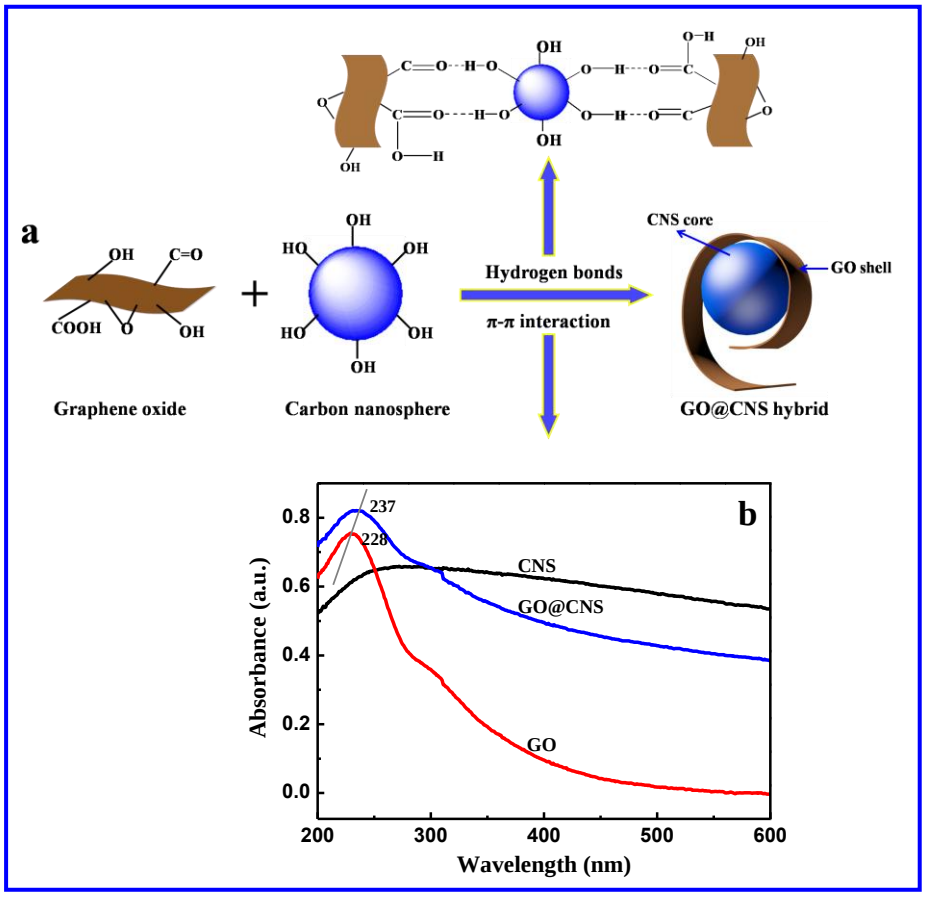

Fig. 2 (a) Schematic illustration of the mechanism for the encapsulating of GO on CNS and (b) UV-vis absorption spectra of GO, CNS and GO@CNS hybrids.

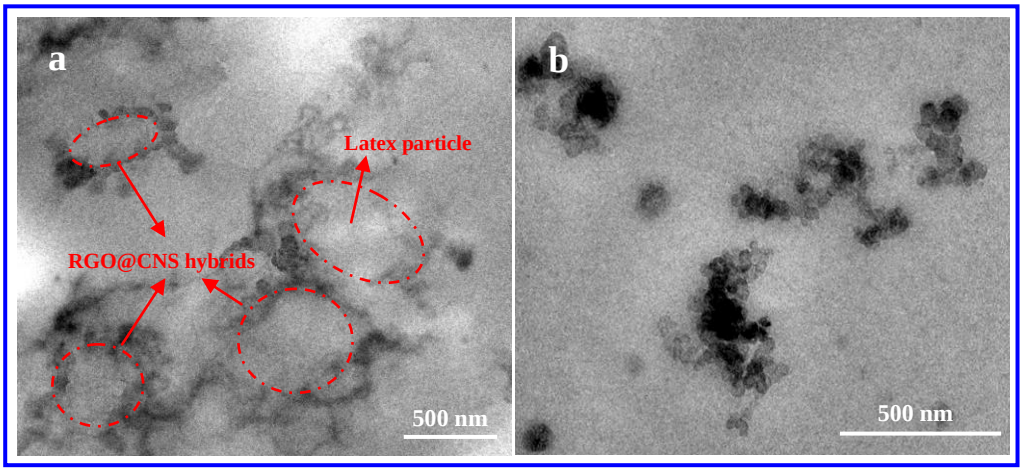

Fig. 3 TEM images of (a) GO@CNS/XNBR composites and (b) CNS/XNBR composite.

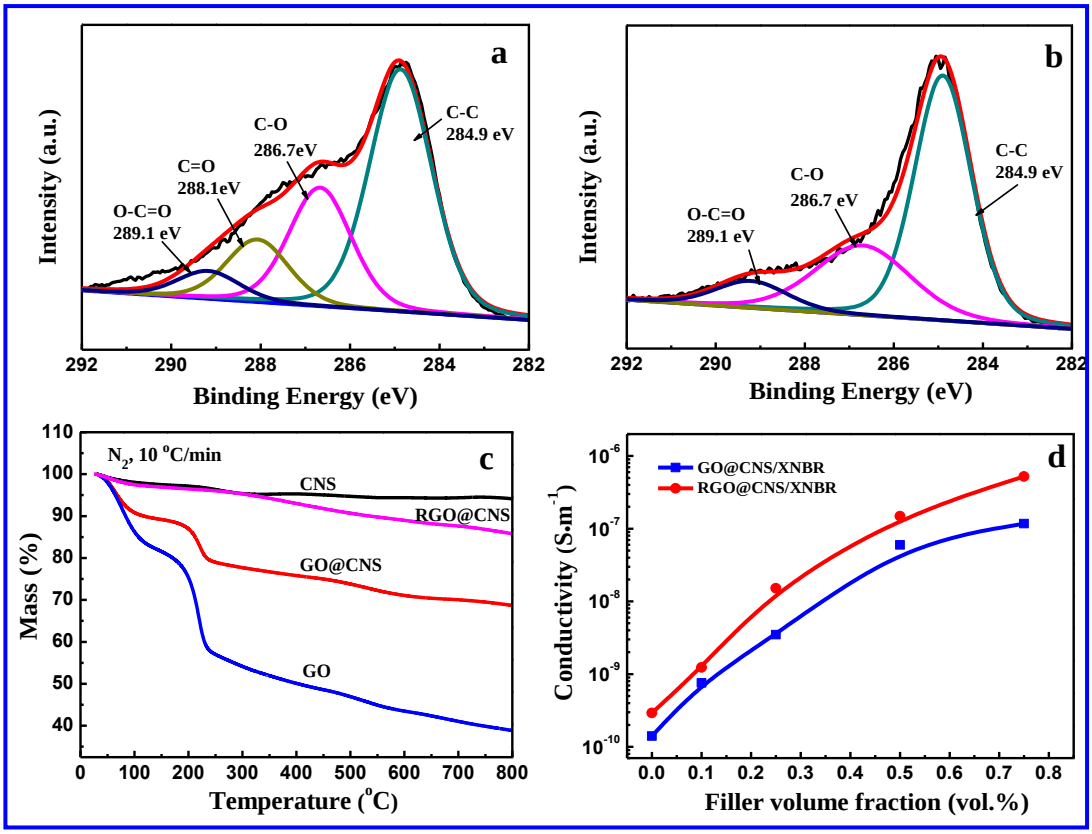

Fig. 4 X-ray photoelectron spectroscopy (XPS) C1s core-level spectra of (a) GO@CNS and (b) RGO@CNS, (c) TGA curves of GO, CNS, GO@CNS and RGO@CNS, and (d) electrical conductivity of GO@CNS/XNBR and RGO@CNS/XNBR composites.

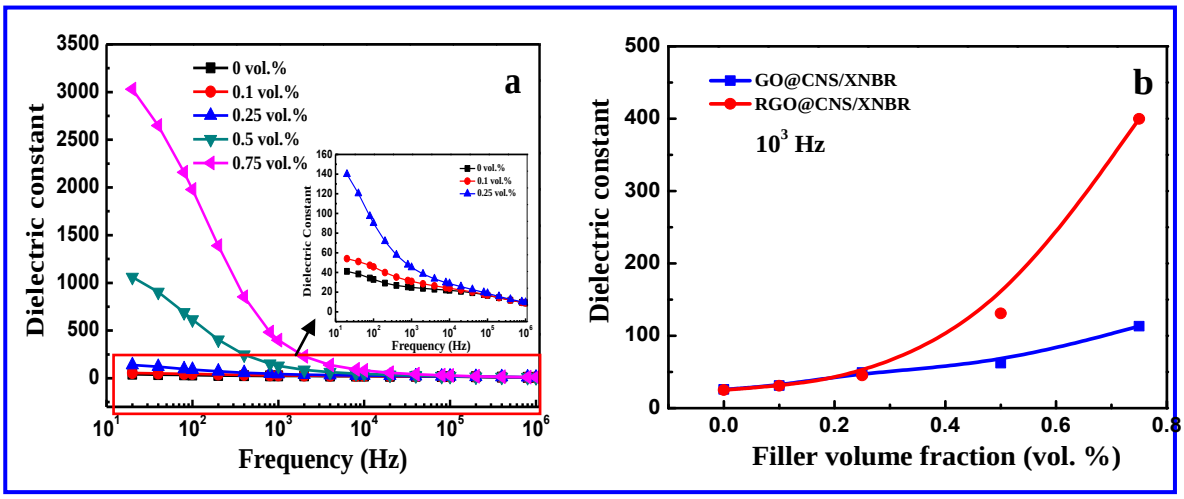

Fig. 5 (a) Frequency response of dielectric constant of RGO@CNS/XNBR composites measured at room temperature, and (b) the dielectric constant of XNBR composites as a function of volume fraction of GO@CNS and RGO@CNS at 10^3 Hz.

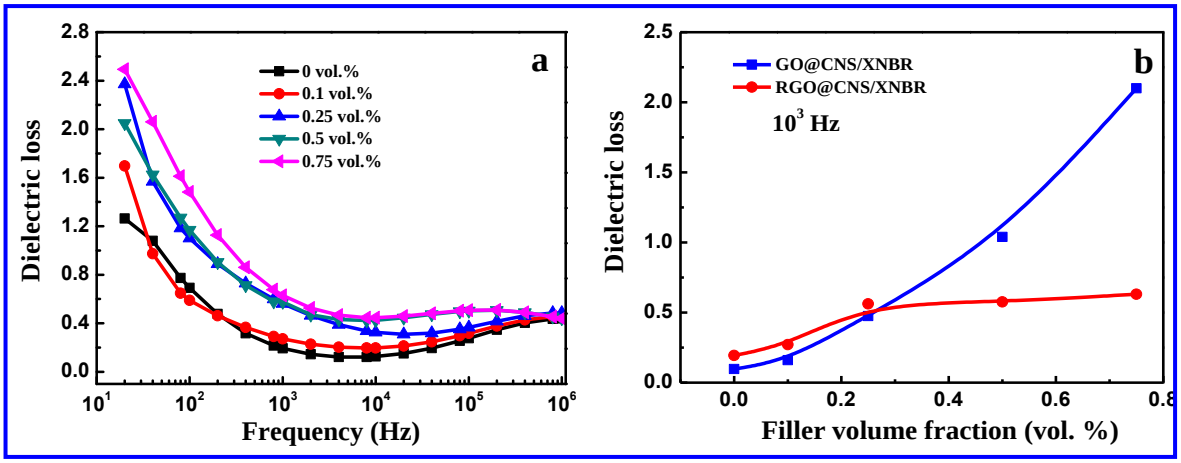

Fig. 6 (a) Frequency response of dielectric loss of RGO@CNS/XNBR composites measured at room temperature, and (b) the dielectric loss of XNBR composites as a function of the volume fraction of GO@CNS and RGO@CNS at 10^3 Hz.

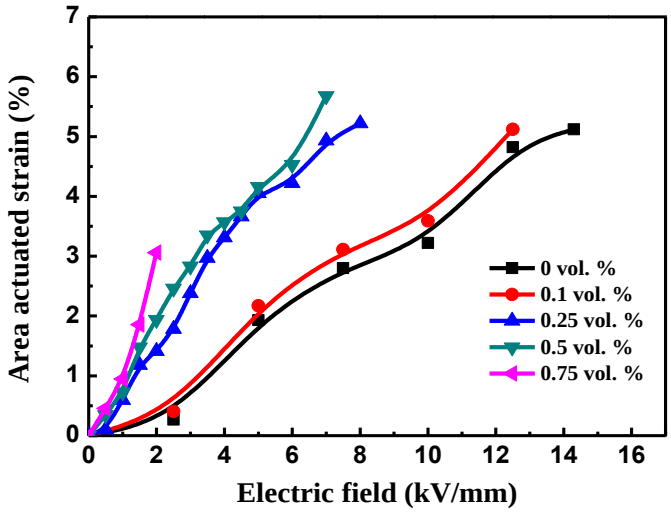

Fig. 7 Actuated strain of XNBR with different contents of RGO@CNS.

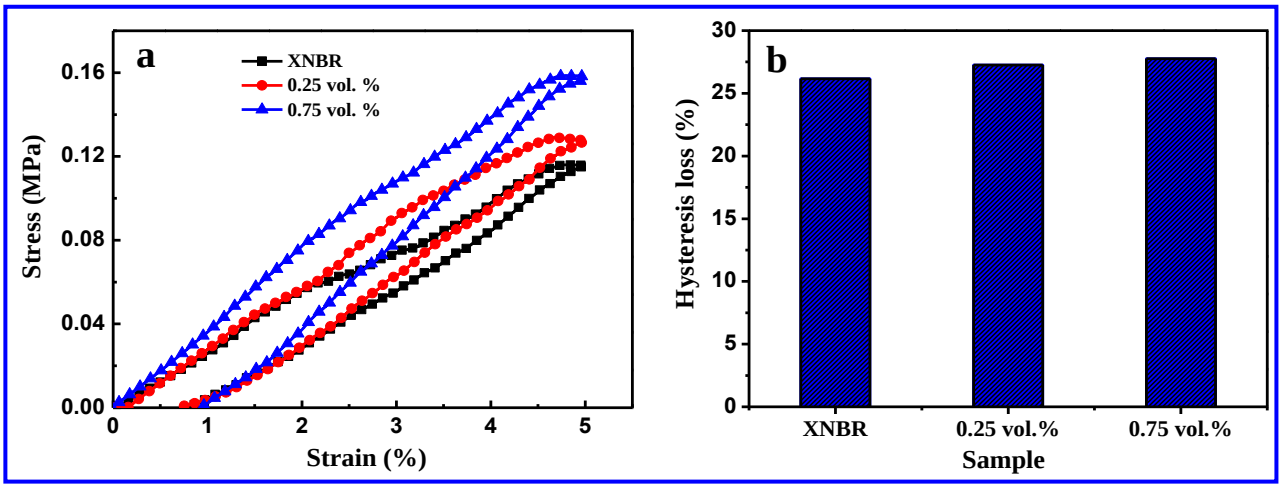

Fig. 8 (a) Strain-stress curve of XNBR and XNBR with 0.25 vol. % and 0.75 vol. % of RGO@CNS; (b) Hysteresis loss of XNBR and XNBR with 0.25 vol. % and 0.75 vol. % of RGO@CNS at 5% strain.

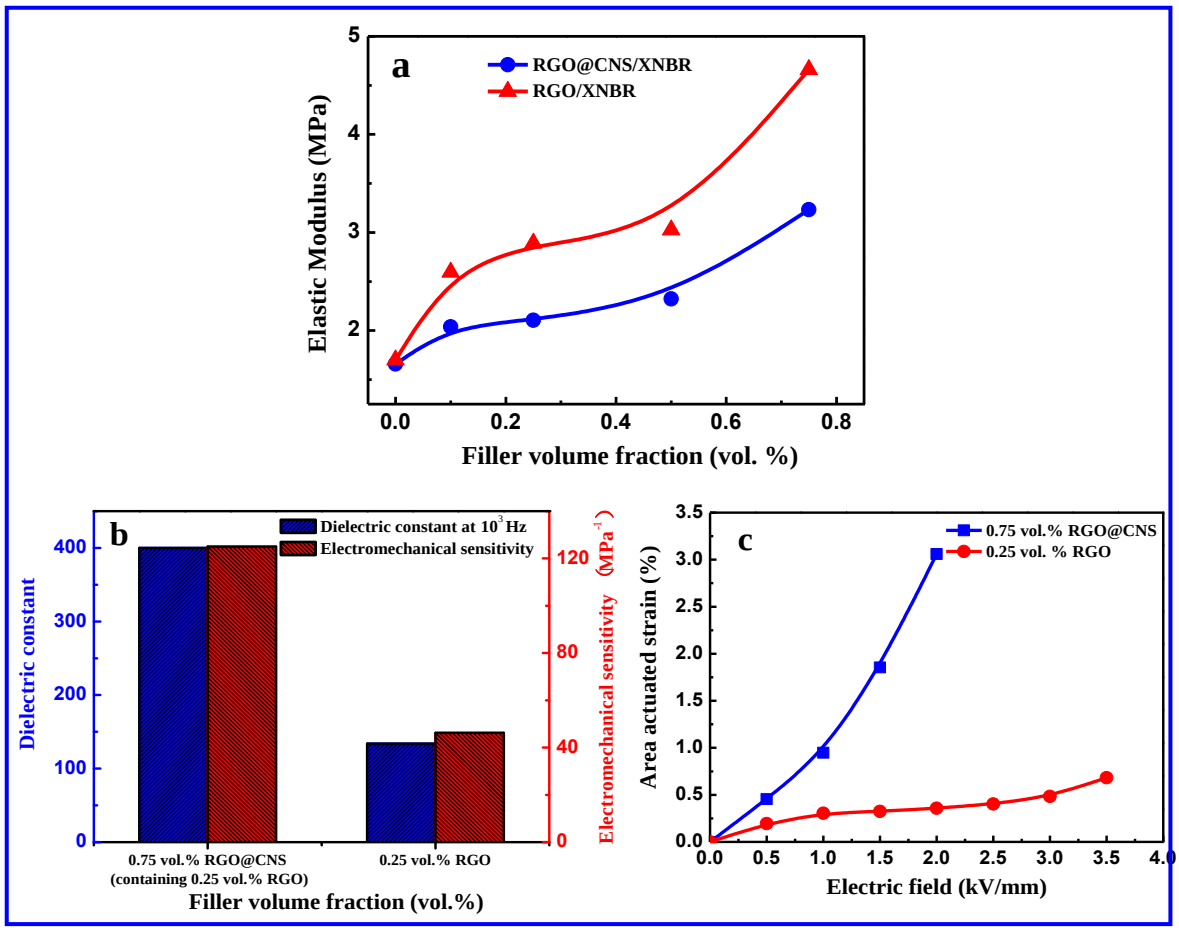

Fig. 9 (a) Plots of elastic modulus of RGO@CNS/XNBR and RGO/XNBR composites against volume fraction of different fillers; (b) Contrast of dielectric constant (k) and electromechanical sensitivity (β) of XNBR composites with 0.75 vol. % of RGO@CNS (containing 0.25 vol. % of RGO) and 0.25 vol. % of RGO at 10^3 Hz; (c) Actuated strain of XNBR with 0.75 vol. % of RGO@CNS (containing 0.25 vol. % of RGO) and 0.25 vol. % of RGO.

High performance dielectric composites by latex compounding of graphene oxide-encapsulated carbon nanosphere hybrids with XNBR

Ming Tian[1, 2], Qin Ma[1], Xiaolin Li[1, 2], Liqun Zhang[1, 2], Toshio Nishi[3], and Nanying Ning[1, 2*]

1. State Key Lab of Organic-Inorganic Composites, Beijing University of Chemical Technology, Beijing 100029, China;
2. Key Laboratory of Carbon Fiber and Functional Polymers, Ministry of Education, Beijing University of Chemical Technology, Beijing 100029, China;
3. Department of Applied Physics, The University of Tokyo, Hongo, Bunkyo-ku, Tokyo, Japan.

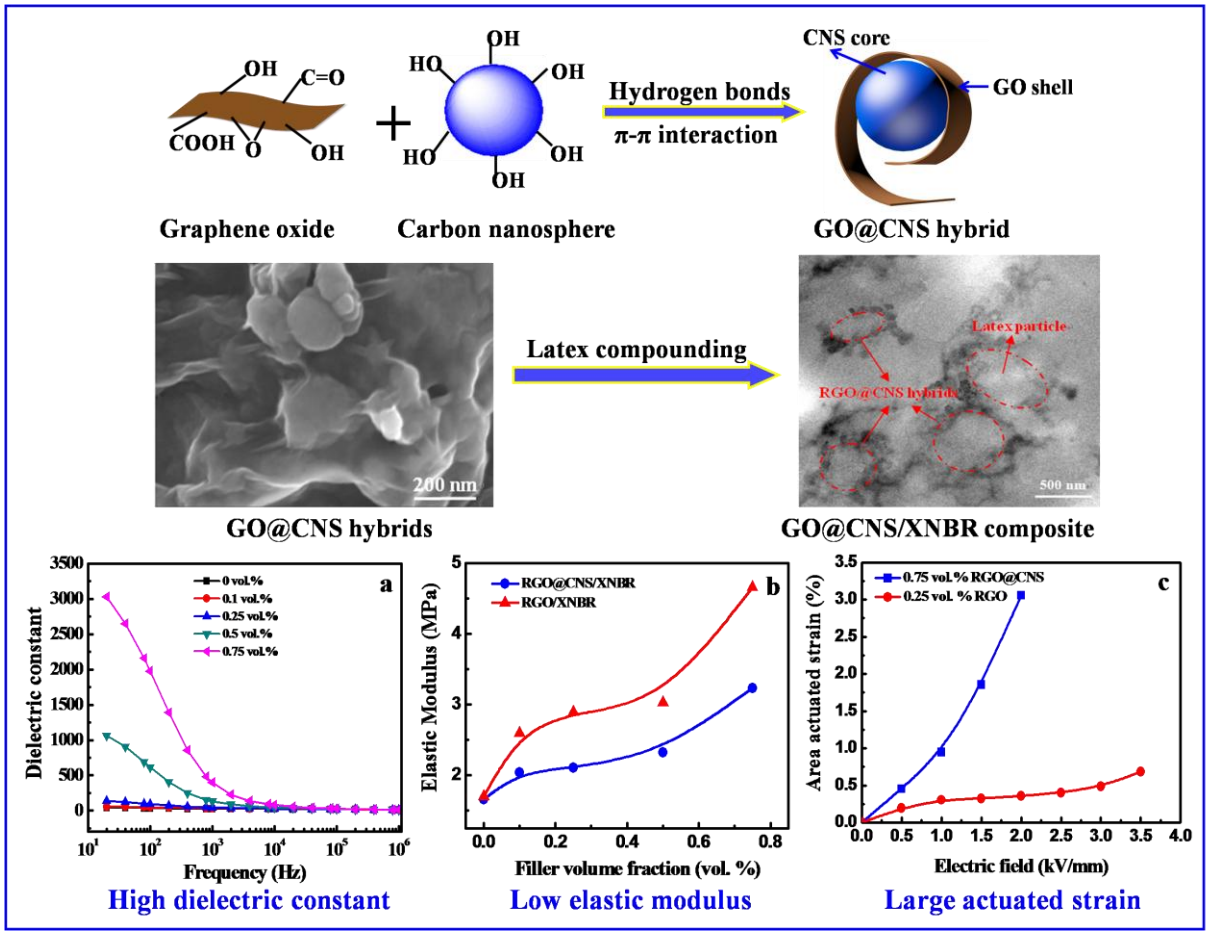

*Corresponding author. E-mail: ningny@mail.buct.edu.cn (N. Ning).